Nanoscale

PAPER

View Article Online
View Journal | View Issue

Cite this: *Nanoscale*, 2023, **15**, 12280

Understanding the Raman enhancement of carbon nanohorns labelled with organic dyes†

Daniel Iglesias, ‡[a,b] Raúl Martín, ‡[a,d] Miguel Á. Álvarez-Sánchez, [a,b] Irene Badía-Domínguez,[c] Ester Vázquez, [a,b] M. Carmen Ruiz Delgado, *[c] Pilar Prieto *[a] and M. Antonia Herrero *[a,b]

Received 23rd March 2023,
Accepted 26th June 2023

DOI: 10.1039/d3nr01357j

rsc.li/nanoscale

Carbon nanohorns have been non-covalently functionalized with two different benzothiadiazoloquinoxalines prepared *via* Stille cross-coupling reactions under solvent-free conditions and microwave irradiation. The close interactions between these organic molecules and the nanostructures resulted in a prominent Raman enhancement, which makes them attractive candidates for multiple applications. A complete experimental physico-chemical characterization has been combined with *in silico* studies to understand these phenomena. The processability of the hybrids was exploited to prepare homogeneous films on substrates with different natures.

Introduction

The unexpected Raman intensity of pyridine adsorbed on silver reported 50 years ago by Fleischman *et al.* set the foundation for the Surface Enhanced Raman Spectroscopy (SERS) field.[1] This is a very active multidisciplinary field that comprises fundamental studies, including *in silico*, to understand this enhancement, the synthesis of high-performing materials, and their development of SERS-based technologies for real-life applications.[2] The narrow spectral bands of Raman spectroscopy, along with its high sensitivity and spatial resolution, are the key advantages for exploiting SERS in sensing and biomedicine.[3] The design and synthesis of SERS tags is fundamental for developing such technologies. These materials must be both high performing, robust and biocompatible and, ideally, should be produced following environmentally friendly methodologies. Most SERS tags are made from nanostructured particles (coated or not) functionalized with small organic molecules used as Raman reporters and eventually with a specific targeting moiety (*e.g.* an antibody).[4] The evolution of nanochemistry has resulted in the synthesis of multiple Raman probes with encouraging results.[3] For instance, Aberasturi *et al.* synthesized star-shaped Au nanoparticles functionalized with several thiolated Raman reporters and coated with an amphiphilic polymer that provided the nanoparticles with long-term stability.[5] The high electromagnetic field localized at the tips of the nanostars produces a large enhancement, which was exploited for cell discrimination in a multiplexed type assay.

Multiplexing is one of the main assets of Raman imaging. This is a major advantage when compared with fluorescence-based techniques, which depends on fluorescent probes with broad emission bands. Given the narrowness of Raman spectral bands, multi-colored images can easily be recorded by monitoring the intensity of two or more vibrations simultaneously. The pallet of colors available using metallic nanoparticles is steading increasing given the numerous research efforts in that field. For instance, Eremina *et al.* sandwiched several small molecules within gold-core silica shell nanoparticles to produce up to 26 different colors.[6] Subsequent bioconjugation of the nanoparticles with different targeting moieties allowed the acquisition multi-colored Raman images *in vivo* and *in vitro*. In contrast, the development of multicolored Raman imaging using carbon nanomaterials is not straightforward. Except for single-walled carbon nanotubes (highly insoluble) and single-layer graphene (only available in substrates and not suitable for imaging), the other known carbon nanoforms (*i.e.* multi-walled carbon nanotubes, graphene oxide, reduced graphene oxide, carbon nanoonions, carbon nanocones and carbon nanohorns) present a very similar Raman fingerprint with two broad bands at *ca.* 1330 cm^{-1} (D-band) and *ca.* 1590 cm^{-1} (G-band). Therefore, it is challenging to achieve multicolor Raman images even by

[a]*Facultad de Ciencias y Tecnologías Químicas, Universidad de Castilla-La Mancha (UCLM), 13071 Ciudad Real, Spain. E-mail: Mariaantonia.herrero@uclm.es*
[b]*Instituto Regional de investigación Científica Aplicada (IRICA), 13071 Ciudad Real, Spain*
[c]*Department of Physical Chemistry, University of Malaga, Campus de Teatinos s/n, Malaga 29071, Spain*
[d]*Instituto de Ciencia de Materiales de Madrid, CSIC Cantoblanco, 28049 Madrid, Spain*

†Electronic supplementary information (ESI) available. See DOI: https://doi.org/10.1039/d3nr01357j

‡These authors contributed equally to this work.

combining several carbon nanostructures. For instance, Liu *et al.* were able to acquire three-colored Raman images by tracking the spectral band of three types of SWCNTs with different isotope compositions.[7] These Raman reporters were synthesized by chemical vapor deposition using ^{13}C-methane, thus highlighting the need for the development of more accessible methodologies to prepare carbon-based multicolor nanotags.

Our group has dedicated intensive research to understanding the Raman enhancement of several oligothiophenes when either adsorbed or covalently grafted to single-walled carbon nanohorns (CNHs).[8,9] CNHs are short single-walled carbon nanotubes that aggregate into spherical particles with a diameter of approximately 100 nm. The properties of CNHs make them very interesting for numerous applications.[10] For example, as they are p-type semiconductors,[11] their large surface area has been exploited for the electrocatalytic production of hydrogen peroxide.[12] In addition, the nanoporosity of N-doped CNHs has been used to encapsulate sulfur to prepare lithium–sulfur batteries with high-performance,[13] and their homogeneous size distribution, absence of metallic particles and low toxicity makes them very interesting in biomedicine.[14] For instance, the photoacoustic effect (*i.e.* emission of sound upon light irradiation) of CNHs has been exploited to image tumors in mice with promising results for image-guided surgery.[15] However, examples of Raman images using CNHs are still scarce, and the access to functionalized carbon nanomaterials for multiplexing is still limited.

In this work, we have synthesized two new nanohybrids comprising pristine CNHs and two different benzothiadiazoloquinoxalines (TDQs) previously reported by some of us (see Fig. 1). Functionalization relies on the non-covalent interaction between the flat aromatic molecules and the large graphitic surface of CNHs. Positions 6 and 7 of the TDQ unit were substituted with either $-CH_3$ or –H groups to understand the importance of CH–π interactions. Note that CH–π interaction, a special sort of hydrogen bonds, can effectively help to establish distinctive self-assembly patterns in organic molecules, thus modulating their resulting photophysical and electronic properties.[16–19] The supramolecular interaction occurs within one hour and requires only straightforward purification with the production of minimal waste. The strong interaction between CNHs and the organic molecules results in the emergence of several Raman bands with potential application in multiplexed Raman imaging. A thorough *in silico* study of the hybrids was carried out to understand this phenomenon. Exploiting the processability of the hybrids, we have prepared homogeneous and continuous sprayed-coated films on different substrates.

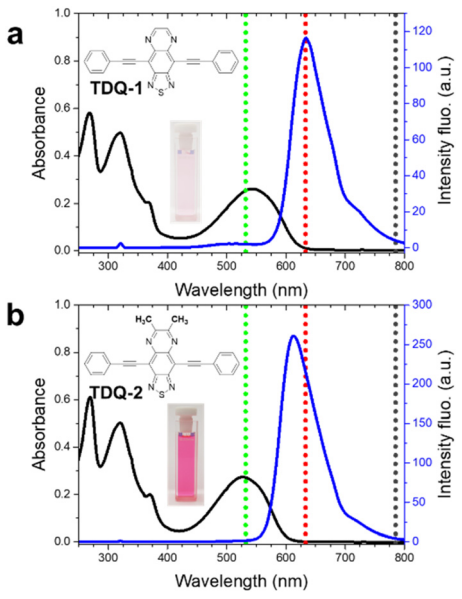

Fig. 1 UV-Vis (black line) and fluorescence spectra (blue line) of **TDQ-1** (a) and **TDQ-2** (b) acquired in $CHCl_3$ (10^{-5} M). The inset illustrates the structure of the molecules and their solution in $CHCl_3$. The dotted lines indicate the wavelength of the laser used for the Raman characterization: green (532 nm), red (633 nm), and grey (785 nm).

Results and discussion

The benzothiadiazole (BTD) core has been extensively used for fluorescence bioimaging,[20] and most recently also for Raman imaging.[21] Oxidation of the BTD core in fuming nitric acid and subsequent iron-catalyzed reduction provides two aromatic amines that are able to react with a dialdehyde to form TDQ units, which have been successfully used for Raman imaging. Qi *et al.* reported an all-in-one organic molecule that can be used for fluorescence, photoacoustic and Raman imaging.[22] These authors exploited the versatility of the molecules encapsulated in polymeric nanoparticles to perform image-guided surgery with encouraging results. The probe consists of a sandwiched donor–acceptor–donor structure, where the donor group is a triphenylamine group and the acceptor is a TDQ core. The TDQ derivative modified with phenyl-alkyne-phenyl units displays an intense Raman band in the cell-silent region at 2215 cm^{-1}. The Raman reporters **TDQ-1** and **TDQ-2** synthesized here represent a minimalist approach with a TDQ core disubstituted with ethynylbenzene groups in positions 4 and 9, respectively (Fig. 1).[23] These groups were added to the TDQ core *via* Stille cross-coupling reactions under solvent-free conditions and microwave irradiation. Further details for the synthesis can be found in the ESI.† The UV-Vis and fluorescence spectra for **TDQ-1** and **TDQ-2** are similar, with both molecules displaying a large absorption band in the visible region centered at 543 and 527 nm for **TDQ-1** and **TDQ-2**, respectively, and an intense red fluorescence emission (633 and 613 nm for **TDQ-1** and **TDQ-2**, respectively). Density functional theory (DFT) calculations showed that the optimized structures present a planar geometry with a HOMO–LUMO gap of 5.26 and 5.36 eV for **TDQ-1** and **TDQ-2**, respectively (Fig. S1†). According to TD-DFT calculations, the lowest energy absorption band is attributed to a one-electron excitation from the HOMO (delocalized over the whole π-conjugated backbone)

to the LUMO (mainly localized over the central TDQ unit), thus displaying an intramolecular charge-transfer (ICT) character (Fig. S1 and S2†). The FT-Raman spectra (λ_{exc} = 1064 nm) for **TDQ-1** and **TDQ-2** as solid powders were recorded (Fig. S3†). Given the good agreement found between the experimental and theoretical Raman spectra, the most relevant Raman features were assigned (Fig. S4 and S5†). The strongest Raman bands, which are collected in the 1600–1200 cm^{-1} region, arise from the strongly mixed CC/CN stretching modes and CH bending vibrations of the whole π-conjugated backbone (see the eigenvectors representation of the involved normal modes in Fig. S6 and S7†).

TDQ-1 and **TDQ-2** were hybridized with pristine CNHs to obtain **CNH-1** and **CNH-2**. Further details can be found in the ESI.† Briefly, a solution of the corresponding TDQ was mixed with a dispersion of CNHs (1 mg ml^{-1} in chloroform) and stirred for one hour. A straightforward purification was required to eliminate the unbound material, which was confirmed by recording the UV-Vis spectra of the washings (Fig. S8†). In contrast to other carbon nanoforms, a brief ultrasonication of CNHs in the appropriate solvent is sufficient to stabilize the suspensions for weeks (Fig. S9†). The quality of these suspensions is key to maximizing the interaction between the dyes and CNHs. Notably, the protocol is sustainable since it requires a minimal energy input, and we were able to recover all the unbound molecules (Fig. S10†).

As seen in Fig. 2, the Raman analysis of all hybrids synthesized display the signals of CNHs (*i.e.* D-, and G-band) and several bands attributed to the organic molecules (see Fig. S11 and S12† for a comparison between the Raman spectra for the hybrids and those of the organic molecules). A comparison of the spectra of **TDQ-1** and **TDQ-2** with those for **CNH-1** and **CNH-2**, clearly shows that the interaction of both dyes with the nanostructure gives rise to a prominent SERS effect, which is stronger for **TDQ-2**.

This suggests an important contribution of the methyl groups in **TDQ-2** compared to **TDQ-1**, which most likely form a greater number of CH–π interactions with the CNH walls. The featureless spectra of **TDQ-1** and **TDQ-2** when irradiated at 532 nm, 633 nm and 785 nm did not allow the enhancement to be quantified (Fig. S13†). The SERS effect can be attributed to electromagnetic enhancement (EE) and chemical enhancement (CE). In addition to EE and CE, the quenching of fluorescence, the energy of the laser, and the interaction of the selected molecule with the substrate play an important role in the process. In this sense, it is very interesting to highlight that the most enhanced Raman bands recorded at around ~850, 1234 and 2190 cm^{-1} corresponds to SN, CC/CN and C≡C stretching modes, respectively, thus reflecting the importance of the interaction between the TDQ core and acetylene groups with the graphitic surface of CNH (see Fig. 2, Fig. S11 and S12†). A complete Raman analysis and fluorescence spectroscopy and *in silico* studies have been carried out to understand this enhancement.

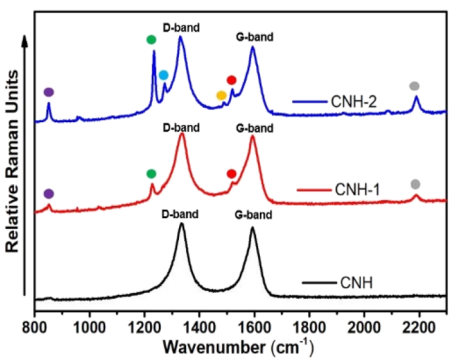

Fig. 2 Raman spectra comparison of the hybrids (**CNH-1** and **CNH-2**) and the pristine CNH. The reported spectra are the average of more than 200 data points acquired after irradiation at 532 nm. The bands highlighted with dotted circles are attributed to the organic molecules (see Fig. S4 and S5† for the vibrational assignment).

The first indication of a CNH-dye interaction was the quenching of fluorescence during the Raman analysis. The fluorescence titration of **TDQ-1** and **TDQ-2** with pristine CNHs revealed a strong quenching of fluorescence for both molecules (Fig. S14†). This is in line with other examples of non-covalent functionalization of nanocarbons with fluorescent molecules.[9,24] It is well known that Raman efficiency depends largely on the energy of the incident light (*i.e.* Raman efficiency $\propto \lambda^{-4}$). **CNH-1** and **CNH-2** were irradiated with three different lasers: green (532 nm), red (633 nm), and infrared (785 nm) at different intensities (Fig. S15†). As expected, the green laser afforded the highest resolution. This laser is in resonance with the lowest energy transition, which corresponds to a HOMO–LUMO one-electron excitation that exhibits ICT character in **TDQ-1** and **TDQ-2** (Fig. 1), which usually increases the efficiency by between two and six orders of magnitude.

In general, the Raman intensity increases gradually with the intensity of the incident light until it reaches a maximum, after which higher intensities would damage the samples. This is not the case for **CNH-1** and **CNH-2** for any of the lasers tested (Fig. S15†). We observed that the signals attributed to the molecular vibrations reach a maximum at 0.1 mW and 0.05 mW for the lasers at 532 and 633 nm, respectively. At higher intensities, the signals of the molecules are hidden by the signal for CNHs. This is due to the asymmetric intensification of the Raman efficiency of the molecule and the nanocarbons upon increasing the intensity of the laser.

The effect of probe concentration on the hybrids was tested. **CNH-1** and **CNH-2** were synthesized by varying the concentration of the probe from 10^{-4} to 10^{-6} M and the optimized conditions (532 nm, 0.1 mW, 4 s) were used to assess this effect. Fig. 3 shows the Raman mappings of the whole set of samples. These data confirm the homogeneity of the enhancement across the samples, which is present in all tested materials. This enhancement decreases gradually with the concentration of the probe. Multiple studies on SERS of graphene and related materials have demonstrated that the enhancement observed is mainly due to the interaction of the first

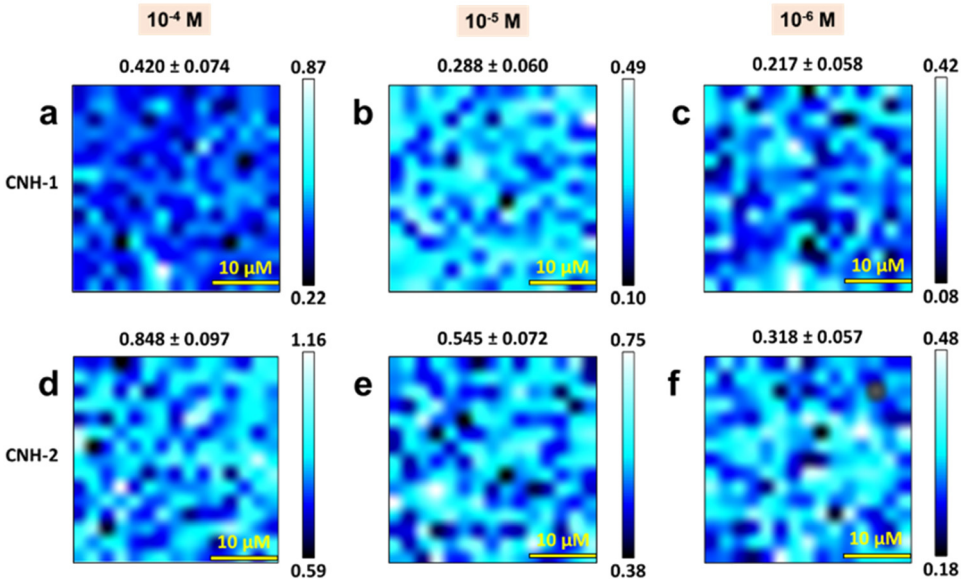

Fig. 3 Raman maps of **CNH-1** (a–c) and **CNH-2** (d–f) showing the intensity at 1227 and 1234 cm^{-1}, respectively. The number on top of each image correspond to the average value with the corresponding standard deviation.

layer of molecules with the substrate.[25,26] The fact that the reported enhancement is larger at high probe concentrations suggests that all conditions tested drive the adsorption of the molecule in a monolayer fashion. This is possible thanks to the large surface area of pristine CNHs (*ca.* 500 m^2 g^{-1}).[27] In addition, the unique petal-like structure might be also responsible for this excellent enhancement since it might possess electromagnetic hot spots for the Raman enhancement as also found in other external petal-like shell structures.[28] Indeed, the effect of similar nano morphologies has also been exploited with gold-based Raman reporters.[5,28]

At this point, we have performed a complete *in silico* study to gain a better understanding of the reported SERS effect and to identify the most favorable configurations of the CNH-dye hybrid and the interactions of **TDQ-1** and **TDQ-2** towards the walls of the CNHs. To this end, eight different adsorption positions of TDQ derivatives on the CNH surface were tested and their total adsorption energies (E_{ads}) were calculated (Fig. S16–S18 and Table S1†). The most favorable CNH-dye arrangements correspond to dispositions *f*–*h* with E_{ads} ranging from −1.80 to −2.09 eV (see Fig. S17, S18 and Table S1†). As seen in Fig. 4 for the most stable disposition *h* taken as a representative example, both TDQ derivatives tend to adapt their molecular structure to maximize the interaction with CNHs *via* non-covalent forces. In fact, combined CH–π and π–π interactions efficiently tether TDQ derivatives to the CNH surface, as we will discuss in detail below. Interestingly, the initial planar TDQ derivatives bend upon adsorption on the CNH surface with a curvature angle of up to 31° (Table S2†).

A careful analysis of the results shows that **TDQ-2** presents a stronger E_{ads} than **TDQ-1**. This can be explained based on the number of CH–π and π–π interactions between the TDQ molecules and the carbon nanohorn: the higher the number

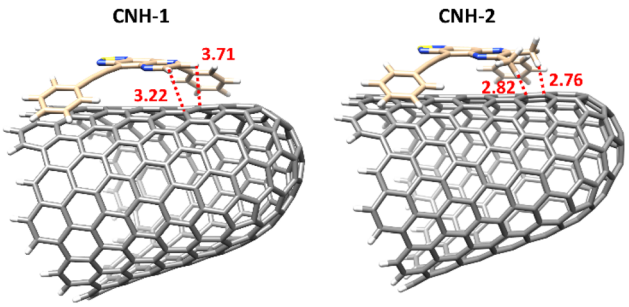

Fig. 4 DFT-optimized (ωB97XD/6-31G**) structures of **CNH-1** and **CNH-2** hybrids in *h* disposition (Fig. S17 and S18† show all different CNH–TDQ dispositions that have been studied). Dotted lines represent the CH–π interactions between the hydrogens of the TDQ unit and the nanohorn in **CNH-1** and **CNH-2**, measured between the corresponding TDQ hydrogens and the shortest neighboring carbon atom of the nanohorn. Distances are given in Angstroms.

of short-distance interactions (*i.e.*, less than 3.3 Å), the stronger the expected adsorption energy. Indeed, the methyl-susbtituted **TDQ-2** possesses more and stronger CH–π interactions with the CNH when compared to the unsubstituted **TDQ-1** (Fig. S19 and Table S3†). Particularly short CH–π interactions (approx. 2.8 Å) are obtained between the hydrogens of the methyl groups in **TDQ-2** and the nanohorn, which might favor the adsorption of derivative **TDQ-2** towards the CNH surface (Fig. 4). This fact might be related with the highest Raman enhancement observed in **CNH-2** when compared to **CNH-1**.

On the other hand, similar HOMO and LUMO topologies, both mainly delocalized over the CNH surface, together with similar HOMO–LUMO gaps were found in the eight conformations of each nanohydrid (Fig. S20 to S22†). This is in consonance with the calculated Mülliken atomic charge distri-

butions (Table S4†) that indicate an absence of charge-transfer character in the ground state of CNH-TDQ hybrids. Although a more detailed inspection of the charge-transfer transitions in the hybrid might be required, the absence of charge-transfer in the ground state suggest that the chemical enhancement could arise from non-resonant changes in the molecular polarizability that might occur upon the dye-CNH hybrid formation.[29–31]

Thus, our theoretical calculations provide the following findings: (i) a combination of CH–π and π–π interactions drives the favorable formation of **CNH-1** and **CNH-2** nanohybrids, (ii) the largest and shortest number of CH–π interactions between the hydrogens of the methyl groups in the TDQ unit and the nanohorn in **CNH-2** seems to be crucial for the selective enhancement of the Raman bands. In summary, the SERS effect probably reflects a complex interplay of both electromagnetic and chemical enhancement mechanisms.[31–33] Although the electromagnetic mechanism might be the dominant contributor to the observed SERS signal enhancement due to the amplification of the electromagnetic fields near the conical-end of CNHs[8] which is also favored by their petal-like structures,[28] the chemical enhancement might also play a role as a result of the short-range dye-CNH interactions.

We have prepared homogeneous and continuous sprayed-coated films on different substrates by exploiting the processability of the hybrids. Numerous applications require the integration of a given functionalized nanomaterial onto substrates of different natures. Here, we exploited the high processability of the synthesized hybrids in organic solvents to prepare homogeneous and continuous films of **CNH-2** by spray-coating (Fig. 5 and Fig. S23†). These films were sprayed on rigid and non-porous materials (*i.e.* glass and Si/SiO_2) and porous and flexible substrates (*i.e.* paper). We also demonstrated that we can create the *ad hoc* designs required for the application by using the proper masks. Subsequently, we confirmed that the SERS effect is preserved after the spray-coating process (Fig. S24†). The electrical characterization of the glass and paper substrates with a four-point probe provided sheet resistance values of 297 kΩ sq^{-1} and 2.96 MΩ sq^{-1}, respectively. Although such high electrical sheet resistances were expected considering the low electrical conductivity of CNHs, they nevertheless indicate that the prepared films are continuous, and that percolation was achieved. These observations were confirmed by SEM (Fig. 5). SEM imaging coupled to an EDS detector confirmed that the hybrids are mainly composed of C (99.8%) with a residual amount of S (0.2%, very close to the limit of detection of the instrument; Fig. S25†). We were not able to detect N atoms using this technique. In addition, the thermogravimetric characterization shows very similar thermograms for pristine CNHs, **CNH-1** and **CNH-2** (Fig. S26†). These finding indicate that the amount of dye adsorbed on the hybrids is rather small, thereby reinforcing the high performance of the SERS effect reported.

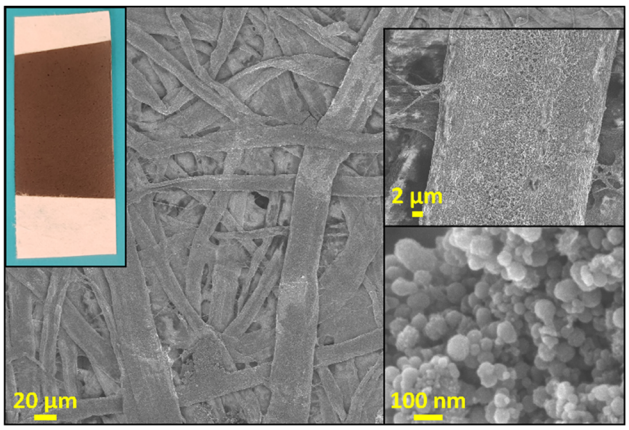

Fig. 5 SEM characterization of a **CNH-2** substrate deposited on paper. The inset pictures show the optical photograph of the substrates and the SEM images at higher magnifications.

Conclusions

We have synthesized two novel hybrid materials combining two *ad hoc* designed TDQs with single-walled carbon nanohorns. A complete physico-chemical characterization including *in silico* studies revealed that a favorable combination of CH–π and π–π drives the formation of the TDQ–CNH nanohybrids. DFT calculations revealed that TDQ molecules bend slightly from their original flat structure to adapt to the curved conical nanomorphology of CNHs. The close interactions between the TDQ and CNH nanostructure result in a significant Raman enhancement of several vibrations related to the SN, CC/CN and C≡C stretching modes of the TDQ core and the acetylene groups. A more prominent SERS signal enhancement is observed when compared unsubstituted **CNH-1** with methyl-substituted **CNH-2** that seems to be closely related to the large number of CH–π interactions in the latter. In addition, we prepared homogeneous **CNH-2** films on a variety of substrates, thereby demonstrating the applicability of the hybrids. The present work represents an important step towards the utilization of functionalized carbon nanomaterials in Raman-based applications. We do hope our findings will inspire other researchers to design carbon-based Raman reporters, which will expand the palette of Raman colors for multiplexed Raman imaging techniques.

Author contributions

M. A. A. performed the experiments. I. B-D. performed the computacional studies. D. I. performed the experiments, wrote the paper, and gave technical suggestions. M. C. R. and P. P. performed the computacional studies, supervised and revised the manuscript. E. V. supervised and revised the manuscript. M. A. H. supervised, reviewed, and edited the manuscript and acquired the principal financial support for the project. All authors approved the final version of the manuscript.

Conflicts of interest

There are no conflicts to declare.

Acknowledgements

DI acknowledges the María Zambrano program under the grant agreement UNI/551/2021. RM acknowledges the Spanish Ministry of Universities for a Margarita Salas postdoctoral fellowship under the agreement UNI/551/2021. Computing Services of University of Castilla-La Mancha and University of Málaga (by the Supercomputing and Bioinformatics center) and IRICA instrumental service are gratefully acknowledged. The work at the University of Málaga was funded by the MICINN (PID2019-110305GB-I00) and by Junta de Andalucía (P09FQM-4708 and P18-FR-4559) projects. The work at the UCLM was funded by the MICINN (PID2020-113080RB-I00, PID2020-119636GB-I00), JCCM (SBPLY/21/180501/000135/1, SBPLY/21/180501/000176, SBPLY/21/180501/000114) projects, DIPUCR-16, L'Oréal/UNESCO Granted and Iberdrola Foundation (CONV120313).

References

1 M. Fleischmann, P. J. Hendra and A. J. McQuillan, *Chem. Phys. Lett.*, 1974, **26**, 163–166.
2 J. Langer, D. J. de Aberasturi, J. Aizpurua, R. A. Alvarez-Puebla, B. Auguié, J. J. Baumberg, G. C. Bazan, S. E. J. Bell, A. Boisen, A. G. Brolo, J. Choo, D. Cialla-May, V. Deckert, L. Fabris, K. Faulds, F. Javier, G. de Abajo, R. Goodacre, D. Graham, A. J. Haes, C. L. Haynes, C. Huck, T. Itoh, M. Käll, J. Kneipp, N. A. Kotov, H. Kuang, E. C. Le Ru, H. K. Lee, J. F. Li, X. Y. Ling, S. A. Maier, T. Mayerhöfer, M. Moskovits, K. Murakoshi, J. M. Nam, S. Nie, Y. Ozaki, I. Pastoriza-Santos, J. Perez-Juste, J. Popp, A. Pucci, S. Reich, B. Ren, G. C. Schatz, T. Shegai, S. Schlücker, L. L. Tay, K. George Thomas, Z. Q. Tian, R. P. van Duyne, T. Vo-Dinh, Y. Wang, K. A. Willets, C. Xu, H. Xu, Y. Xu, Y. S. Yamamoto, B. Zhao and L. M. Liz-Marzán, *ACS Nano*, 2020, **14**, 28–117.
3 J. Plou, P. S. Valera, I. Garc, C. D. L. De Albuquerque, A. Carracedo and L. M. Liz-marz, *ACS Photonics*, 2022, **9**, 333–350.
4 Y. Li, Z. Wang, X. Mu, A. Ma and S. Guo, *Biotechnol. Adv.*, 2017, **35**, 168–177.
5 D. J. De Aberasturi, A. B. Serrano-montes, J. Langer, M. Henriksen-lacey, W. J. Parak and L. M. Liz-marza, *Chem. Mater.*, 2016, **28**, 6776790.
6 O. E. Eremina, A. T. Czaja, A. Fernando, A. Aron, D. B. Eremin and C. Zavaleta, *ACS Nano*, 2022, **16**, 10341–10353.
7 Z. Liu, X. Li, S. M. Tabakman, K. Jiang, S. Fan and H. Dai, *J. Am. Chem. Soc.*, 2008, **130**, 13540–13541.
8 D. Iglesias, J. Guerra, M. I. Lucío, R. C. González-Cano, J. T. López Navarrete, M. C. Ruiz Delgado, E. Vázquez and M. A. Herrero, *Chem. Commun.*, 2020, **56**, 8948–8951.
9 D. Iglesias, J. Guerra, M. V. Gómez, A. M. Rodríguez, P. Prieto, E. Vázquez and M. A. Herrero, *Chem. – Eur. J.*, 2016, **22**, 11643–11651.
10 N. Karousis, I. Suarez-martinez, C. P. Ewels and N. Tagmatarchis, *Chem. Rev.*, 2016, **116**, 4850–4883.
11 A. Zieleniewska, F. Lodermeyer, M. Prato, G. Rumbles, D. M. Guldi and J. L. Blackburn, *J. Mater. Chem. C*, 2022, **10**, 5783–5786.
12 D. Iglesias, A. Giuliani, M. Melchionna, S. Marchesan, A. Criado, L. Nasi, M. Bevilacqua, C. Tavagnacco, F. Vizza, M. Prato and P. Fornasiero, *Chem*, 2018, **4**, 106–123.
13 U. Gulzar, T. Li, X. Bai, M. Colombo, A. Ansaldo, S. Marras, M. Prato, S. Goriparti, C. Capiglia and R. P. Zaccaria, *ACS Appl. Mater. Interfaces*, 2018, **10**, 5551–5559.
14 J. Guerra, M. A. Herrero and E. Vázquez, *RSC Adv.*, 2014, **4**, 27315–27321.
15 D. Li, Y. Zhang, J. Xu, F. Yoshino, H. Xu, X. Chen and L. Zhao, *Carbon*, 2021, **180**, 185–196.
16 A. Benito-Hernández, U. K. Pandey, E. Cavero, R. Termine, E. M. García-Frutos, J. L. Serrano, A. Golemme and B. Gómez-Lor, *Chem. Mater.*, 2013, **25**, 117–121.
17 C. Ruiz, U. K. Pandey, R. Termine, E. M. García-Frutos, G. López-Espejo, R. P. Ortiz, W. Huang, T. J. Marks, A. Facchetti, M. C. Ruiz Delgado, A. Golemme and B. Gómez-Lor, *ACS Appl. Mater. Interfaces*, 2016, **8**, 26964–26971.
18 H. Wu, P. Zhao, X. Li, W. Chen, H. Ågren, Q. Zhang and L. Zhu, *ACS Appl. Mater. Interfaces*, 2017, **9**, 3865–3872.
19 N. Suzuki, T. Matsuda, T. Nagai, K. Yamazaki and M. Fujiki, *Cryst. Growth Des.*, 2016, **16**, 6593–6599.
20 B. A. D. Neto, P. H. P. R. Carvalho and J. R. Correa, *Acc. Chem. Res.*, 2015, **48**, 1560–1569.
21 K. Cui, Y. Zhang, G. Chen, Y. Cui, W. Wu, N. Zhao, T. Liu and Z. Xiao, *Small*, 2022, **18**, 1–9.
22 J. Qi, J. Li, R. Liu, Q. Li, H. Zhang, J. W. Y. Lam, R. T. K. Kwok, D. Liu, D. Ding and B. Z. Tang, *Chem*, 2019, **5**, 2657–2677.
23 R. Martín, P. Prieto, J. R. Carrillo, A. M. Rodríguez, A. De Cozar, P. G. Boj, M. A. Díaz-García and M. G. Ramírez, *J. Mater. Chem. C*, 2019, **7**, 9996–10007.
24 G. Pagona, A. S. D. Sandanayaka, A. Maignø, J. Fan, G. C. Papavassiliou, I. D. Petsalakis and B. R. Steele, *Chem. – Eur. J.*, 2007, **13**, 7600–7607.
25 S. Feng, M. C. Santos, B. R. Carvalho, R. Lv, Q. Li, K. Fujisawa, A. L. Elías, Y. Lei, N. Perea-López, M. Endo, M. Pan, M. A. Pimenta and M. Terrones, *Sci. Adv.*, 2016, **2**, 1–13.
26 X. Ling and J. Zhang, *Small*, 2010, **6**, 2020–2025.
27 S. Utsumi, J. Miyawaki, H. Tanaka, Y. Hattori, T. Itoi, N. Ichikuni, H. Kanoh, M. Yudasaka and S. Iijima, *J. Phys. Chem. B*, 2005, **109**, 14319–14324.
28 Y. Zhang, Y. Gu, J. He, B. D. Thackray and J. Ye, *Nat. Commun.*, 2019, **10**, 3905.
29 A. Campion, P. Kambhampati, A. Campion and C. Harris, *Chem. Soc. Rev.*, 1998, **27**, 241–250.

30 S. M. Morton, D. W. Silverstein and L. Jensen, *Chem. Rev.*, 2011, **111**, 3962–3994.
31 D. J. Trivedi, B. Barrow and G. C. Schatz, *J. Chem. Phys.*, 2020, **153**, 124706.
32 B. J. Schwartz, *Annu. Rev. Phys. Chem.*, 2003, **54**, 141–172.
33 M. Yilmaz, M. Ozdemir, H. Erdogan, U. Tamer, U. Sen, A. Facchetti, H. Usta and G. Demirel, *Adv. Funct. Mater.*, 2015, **25**, 5669–5676.